LAWRENCE
LIVERMORE
NATIONAL
LABORATORY

LLNL-JRNL-409685

The role of parallel heat transport in the relation between upstream scrape-off layer widths and target heat flux width in H-mode plasmas of NSTX.

J. W. Ahn, J. A. Boedo, R. Maingi, V. A. Soukhanovskii

January 7, 2009

Physics of Plasmas

Disclaimer

The role of parallel heat transport in the relation between upstream scrape-off layer widths and target heat flux width in H-mode plasmas of National Spherical Torus Experiment

J-W. Ahn[1], J. A. Boedo[1], R. Maingi[2], V. Soukhanovskii[3], and the NSTX Research Team

[1]University of California – San Diego, San Diego, CA 92093, USA

[2]Oak Ridge National Laboratory, Oak Ridge, TN 37831, USA

[3]Lawrence Livermore National Laboratory, Livermore, CA 94551, USA

Abstract

The physics of parallel heat transport was tested in the Scrape-off Layer (SOL) plasma of the National Spherical Torus Experiment (NSTX) [M. Ono, *et al*., Nucl. Fusion **40**, 557 (2000) and S. M. Kaye, *et al*., Nucl. Fusion **45**, S168 (2005)] tokamak by comparing the upstream electron temperature (T_e) and density (n_e) profiles measured by the mid-plane reciprocating probe to the heat flux ($q_\perp$) profile at the divertor plate measured by an infrared (IR) camera. It is found that electron conduction explains the near SOL width data reasonably well while the far SOL, which is in the sheath limited regime, requires an ion heat flux profile broader than the electron one to be consistent with the experimental data. The measured plasma parameters indicate that the SOL energy transport should be in the conduction-limited regime for R-R_{sep} (radial distance from the separatrix location) < 2-3 cm. The SOL energy transport should transition to the sheath-limited regime for R-R_{sep} > 2-3cm. The T_e , n_e , and $q_\perp$ profiles are better described by an offset exponential function instead of a simple exponential. The conventional relation between mid-

plane electron temperature decay length (λ_{Te}) and target heat flux decay length (λ_q) is λ_{Te}=7/2λ_q, whereas the newly-derived relation, assuming offset exponential functional forms, implies λ_{Te}=(2-2.5)λ_q. The measured values of λ_{Te}/λ_q differ from the new prediction by 25~30%. The measured λ_q values in the far SOL (R-R_{sep} > 2-3cm) are 9-10cm, while the expected values are 2.7 < λ_q < 4.9 cm (for sheath-limited regime). We propose that the ion heat flux profile is substantially broader than the electron heat flux profile as an explanation for this discrepancy in the far SOL.

I. Introduction and background

The Scrape-off Layer (SOL) heat flux decay length at the divertor target, λ_q, in tokamak plasmas is an important parameter related to the effective surface area over which power from the core plasma is distributed in the heat strike regions at the target. This impacts choices of target material, shape, and the upper limit of the heat flux to avoid material damage. Therefore, a thorough understanding of the transport mechanisms that set λ_q is critical for the next generation devices, such as ITER[1, 2].

There have been a number of efforts to scale experimentally observed λ_q values with plasma operation parameters such as $\bar{n}_e$, B_t, q_{95}, and input power as well as to compare them with theoretical models. Such early works were summarized by Connor and Counsell[3] which identified a group of better fitting models against the experimental data. The theoretical models are derived from choices of given physics basis for perpendicular heat diffusivity, $\chi_\perp$, and the use of parallel and perpendicular power balance equations. Although there have been several attempts[4, 5] to extrapolate fitting results to future machines, there is still a strong need for verification, improved experimental measurements, and a theory-oriented approach for the extrapolation.

On the other hand, the dependence of λ_q on the upstream plasma parameters is directly related to the parallel heat transport process and can vary significantly with the SOL plasma conditions due to different energy transport regimes. It is the relationship of λ_q with temperature and density decay lengths, λ_T and λ_n, that can shed light on the parallel heat transport mechanisms and is the topic of investigation in this paper.

The competition between parallel and perpendicular transport processes determines the SOL cross-field scale lengths. It is generally accepted that most of the target plate heat flux can be explained by electron conduction in attached plasmas and by ion convection during detachment[6, 7], with some noteworthy exceptions[8, 9].

In attached plasmas with electron conduction dominating ion transport, heat transport parallel to the magnetic field can be written as:

$$q_{\parallel} \approx q_{\parallel}^{e} = -\kappa_0 T_e^{5/2} \frac{dT_e}{ds_{\parallel}} \qquad (1)$$

where $s_{\parallel}$ is the parallel coordinate and κ_0 is the electron conduction coefficient. This equation can be integrated along the SOL to give a well-known expression for the upstream electron temperature, $T_{e,u}$,

$$T_{e,u} \sim \left(\frac{7}{2} \frac{q_{\parallel} L_c}{\kappa_0} \right)^{2/7} \qquad (2)$$

where L_c is the parallel connection length. This simplified picture of SOL transport is referred to as the two-point model, for which a detailed discussion can be found elsewhere[10, 11, 12]. Assuming further that the T_e and $q_{\parallel}$ profiles are simple exponentials gives a simple relation between power and temperature perpendicular decay lengths,

$$\lambda_{Te,u} = \frac{7}{2} \lambda_q \qquad (3)$$

This relation has been previously used, for example, to obtain upstream T_e from the measured target λ_q or to translate λ_{Te} into the target λ_q[13, 14].

However, recent studies have shown that fast, intermittent cross-field transport leads to flat T_e and n_e profiles in the far SOL[15, 16]. The profile shapes then appear as exponentials with a baseline offset, instead of simple exponentials. Recall that the relation between λ_{Te} and λ_q given in equation 3 assumes that parallel heat conduction dominates energy transport, leading to simple exponential radial profiles. Thus the consideration of intermittent radial transport and offset-exponential plasma profiles will lead to a modification of the relationship given in equation 3. In the remainder of this paper we will compare the experimental ratio of λ_{Te}/λ_q to that given in equation 3, and a new ratio based on offset exponential profile forms.

II. Results and Data Analysis

A. Measurement of SOL Plasma Profiles

Experiments to obtain the ratio of plasma cross-field scale lengths were performed in the National Spherical Tokamak Experiment (NSTX)[17, 18] (R = 0.85 m, a < 0.67 m, R/a > 1.27) in lower single null (LSN) discharges, with toroidal magnetic field, B_T = 0.5 T, plasma current, I_p = 0.8 – 1MA, line average electron density $\overline{n}_e = 4.0\times10^{19}$ m^{-3}, and neutral beam injected (NBI) power of 1 MW. Simultaneous measurements of the upstream T_e and the target $q_\perp$ profiles were made using a fast reciprocating probe[19] and infra-red (IR) camera[20], respectively, in quiescent H-mode plasmas with small, Type-V ELMs[21]. The fast reciprocating probe measures upstream plasma parameters (17.3 cm below the mid-plane) across the SOL with spatial resolution of 1 – 2mm. The IR camera measures tile surface emissivity, which is converted to tile surface temperature from in-situ calibration during baking of the graphite tiles. The target heat flux profile is obtained from a 1-D solution of the conduction equation with temperature independent thermal properties[22], with temporal resolution of ~33 ms and spatial resolution of ~6 mm. The

geometry of the two diagnostics is shown in Fig. 1 as well as the magnetic equilibrium reconstruction for shot 125059. Data from both diagnostics is mapped to the outer midplane using equilibrium reconstructions[23, 24].

Fig. 2 shows the time evolution of a) plasma current (I_p), b) line averaged density ($\bar{n}_e$), c) injected neutral beam power (P_{NBI}), and d) D_α signal for lower divertor, for shot 125069 and indicates the time window during which probe and IR measurements are taken. The L-H transition is indicated by the D_α drop at 190ms, and the plasma stays in H-mode until ~ 430ms. The small oscillations on D-alpha are signatures of the Type-V ELMs. Note also the continuous rise of the line-averaged density during this time period, a common feature of NSTX H-modes. Note also the NBI waveform: a relatively high power level of 4 MW was used to trigger a reproducible L-H transition, and this power level was reduced in steps as the target line-average density for the reciprocating probe plunge was achieved.

The time dependent measurements during the probe plunge are converted to spatial profiles using mapping based on equilibrium reconstructions. In this manner, several ion saturation current density (j^+_{sat}) profiles, as a function of R-R_{sep} (mapped to the mid-plane), are shown in Fig. 3 for four nominally identical discharges. It is noted that the profiles are quite reproducible, indicating that the SOL plasma characteristics for these discharges are comparable. The discharge with the deepest probe plunge was chosen for the data analysis.

High spatial resolution profiles of T_e and n_e as measured by the fast probe are shown in Fig. 4, as well as the heat flux profile inferred from the IR camera emissivity data. Note that we plot a different discharge from the ones in Fig. 3 because the j^+_{sat} data is best for 125069 (see discussions in section III). Systematic error bars on the heat flux measurements are difficult to estimate because of approximations in the conduction model and possible tile emissivity variations between the in-situ calibration and the experiment. However the statistical error bars

are less than 10%. Also shown in Fig. 4 are statistical error bars on the fits of T_e, n_e, and heat flux profiles.

Notice that the T_e profile in Fig. 4 shows a significant scatter. This is believed to be due to the disturbance of small ELMs and turbulent blobs to the SOL plasma during the measurement. Specifically, the T_e is essentially determined by the slope of the I-V characteristic; small ELMs cause a substantial temporary change to the slope, thus affecting the fitted T_e values. In contrast, the n_e is determined mostly by the fitted ion saturation current value, which is less affected by small ELMs. A more detailed discussion for the effect of ELMs and turbulent blobs on the T_e profile is given in section III.

The electron-electron collisionality ($\nu^*_{ee} = L_c/\lambda_{ee}$, where λ_{ee} is the *e*-*e* mean free path and L_c is the parallel connection length) in the upstream SOL region was calculated from the T_e and n_e profile data and L_c calculated by LRDFIT magnetic equilibrium reconstruction[25], to determine the SOL heat flow regime (*i.e.*, conduction-limited, sheath-limited, or detached).

B. Categorization of SOL Plasma Regimes

It is seen from Fig. 4 that the plasma is strongly collisional with ν^*_{ee} of ~30 near R-R_{sep} = 0 and ν^*_{ee} rapidly decreases away from the separatrix to ~5 at R-R_{sep} = 8cm. This indicates that the SOL plasma is in the conduction-limited regime near the separatrix and in the sheath-limited regime near the wall. Also, there are representative upstream parameters[12, 26], relating the upstream plasma conditions (T_u and n_u) to the conditions required for transition from the conduction-limited regime to the sheath-limited or detachment regimes given by:

$$T_u\big|_{cond\Leftrightarrow sh} \approx 3.2\times10^{-9}\left(n_u L_c\right)^{1/2} \qquad (4)$$

$$T_u\big|_{cond\Leftrightarrow \det} \approx 1.1\times10^{-9}\left(n_u L_c\right)^{1/2} \qquad (5)$$

These relations are plotted on a T_{eu} *vs* $(n_{eu}L_c)^{1/2}$ plane in Fig. 5 to show the boundaries of the various regimes, using the same probe data shown in Fig. 4. The profile data indicates that the near SOL plasma (R-R_{sep} < 3cm) should be in the conduction-limited regime, while the far SOL plasma (R-R_{sep} > 3cm) should be in the sheath-limited regime. One implicit assumption here is that the radiation loss in the divertor region is small. Divertor bolometry data, although sparse, suggests a radiation loss in the divertor region of only ~70 kW compared to a total of ~310 kW deposited on the outer lower divertor plates as per the IR camera (see section II.D for more detailed discussion). We will therefore neglect it for now, but come back to this point later.

C. Analysis of Near SOL Widths

We have established that the probe profile in the near SOL is in the conduction-limited regime, and therefore equation 3 relating the T_e and q decay lengths should hold in this region. We can now compare experimental IR camera data of λ_q with mid-plane probe data (T_e and n_e). One initial observation by examining Fig. 4 is that the T_e, q, and n_e profiles do not follow a simple exponential decay, but have a long tail in the far SOL region. The near SOL T_e and q decay lengths are obtained by fitting the data to a simple exponential function for 0 < R-R_{sep} < 2.5cm, indicated by orange lines in Fig. 4, yielding λ_{Te} = 2.3 cm and λ_q = 1.0 cm and therefore λ_{Te}/λ_q = 2.3. The expected ratio is 3.5 from equation 3, *i.e.* the difference is 34%. This indicates that the SOL profiles in this region can be roughly described by classical transport processes.

The long tail in the far SOL region can be approximated as an offset in the exponential function, $a = a_0 + a_1 \exp\left(-\frac{R - R_{sep}}{\lambda_a}\right)$ which can be used to fit the T_e, n_e, and q profiles (black solid lines in Fig. 4). This alternate function yields a shorter decay length in the near SOL region, as compared to the simple exponential fit. The resulting λ_{Te}/λ_q ratio of 1.52 is significantly smaller than the

expected ratio of 3.5. However, the 7/2 ratio is based on the simple exponential decay length for both T_e and q. If we use the offset exponential function for both T_e and q profiles and apply it to equation 2, we obtain a new relation between λ_{Te} and λ_q,

$$\lambda_{Te,u} = \frac{7}{2}\lambda_q\left(\frac{T_{e,u} - T_{e0}}{T_{e,u} - Cq_0 T_{e,u}^{-5/2}}\right) \qquad (6)$$

where, $C = \frac{7}{2}\frac{L_c}{\kappa_0}$, T_{e0} and q_0 are the offset T_e and q values. If we apply this relation to the near SOL region for the example in Fig. 4, while taking $T_{e,u}$ as a line-averaged value, $T_{e,u} = \frac{\int T_e(r)dr}{\int dr}$, the factor $\frac{T_{e,u} - T_{e0}}{T_{e,u} - Cq_0 T_{e,u}^{-5/2}}$ is 0.59. Thus the expected λ_{Te}/λ_q ratio drops to 2.05, which is in reasonable agreement with the measured value of 1.52 with the offset exponential fitting. The use of offset temperature and heat flux values, T_{e0} and q_0, in the parallel conduction equation (equation 2) can be interpreted as a representation of relatively strong perpendicular convection.

The above analysis was completed for two additional Type-V ELMy H-mode discharges with different plasma currents. Fig. 6 shows a comparison of λ_{Te}/λ_q values between the experiment and the conduction model for all three discharges. It is seen that the experimental λ_{Te}/λ_q values are generally smaller than those from parallel electron conduction model. Simple exponential fittings for experimental data produce average λ_{Te}/λ_q = 2.67±0.81cm, compared to 3.5 from the two-point model. Offset exponential fittings for experimental data give average λ_{Te}/λ_q = 1.63±0.13cm, compared to 2.25±0.26cm from the modified two-point model (equation 6). In both cases, the experimental values are 25-30% smaller than theoretical predictions, suggesting that other processes may also play a role in parallel heat transport in the near SOL.

D. Analysis of Far SOL Widths

The far SOL plasma (R-R_{sep} > 2.5cm) is in the sheath-limited regime according to the conventional regime categorization (see Fig. 5) and the electron and ion energy balance equation, $q_{\parallel}^{e,i} = \frac{1}{2} n c_s \gamma_s^{e,i} k T_{e,i}$, gives a simple relation between various decay lengths in the sheath-limited regime[10, 12], again assuming a simple exponential decay length for each profile,

$$\frac{1}{\lambda_q^{e,i}} = \frac{1}{\lambda_{ne,i}} + \frac{3}{2\lambda_{Te,i}} \qquad (7)$$

We can test this relation by fitting the T_e, n_e, and q profiles in the region R-R_{sep} > 2.5cm to the simple exponential function, which yields λ_{Te} =12.7 cm, λ_{ne}=3.9 cm, and λ_q=9.3 cm (shown in Fig. 4 with blue lines). Equation 7 above yields λ_q^e value of 2.7 cm. Although ion temperature (T_i) is not measured for NSTX SOL plasmas, there is a tendency of $T_i^{SOL} > T_e^{SOL}$ [27, 28] and $\lambda_{Ti}^{SOL} \to \infty$ [12]. This gives λ_q^i value of 3.9 cm from equation 7, assuming equal electron and ion densities and therefore $\lambda_{ne} = \lambda_{ni}$. As the measured IR heat flux is a combination of electron and ion contributions ($q_{\parallel} = q_{\parallel}^e + q_{\parallel}^i$), λ_q is $\lambda_q^e < \lambda_q < \lambda_q^i$. It is therefore expected that 2.7 < λ_q < 3.9 cm. The actual measurement is λ_q =9.3 cm, a factor of 2.4 – 3.4 longer than the expected value. Furthermore, the conduction limited regime would predict a λ_q value of 3.6 cm (equation 3) in the far SOL, again a factor of 2.6 smaller than the measured value. All the results for the near and far SOL widths for shot 125069 (Fig. 4) are summarized in TABLE 1.

TABLE 1. λ_{Te}/λ_q ratio for the near SOL and λ_q for the far SOL, for shot 125069 in Fig. 4

	Measurement by fitting to profile		***Prediction from two-point model using,***	
	Simple exponential	**Offset exponential**	**Simple exponential**	**Offset exponential**
λ_{Te}/λ_q in near SOL	2.30±0.11	1.52±0.08	3.5	2.05
λ_q in far SOL	9.3±0.7cm	–	2.7–3.9cm	–

There are several possible explanations for the long λ_q observed in the far SOL. The first concerns the model used to infer heat flux from IR camera emissivity measurements. The IR camera technically measures surface thermal emission, which is converted to temperature from a calibration during an in-situ bake of the graphite tiles. There could be differences in the tile surface film characteristics from the time of the bake to the plasma experiments, due to plasma-wall interactions and/or surface coating of the graphite by boronization to improve plasma performance. Comparison of daily standard discharges indicates that this effect is minor at the outer strike point, typically a region of high heat flux and net erosion. Another possibility to consider for the IR heat flux data is that the 1-D conduction model used to convert surface temperature to heat flux is over-simplified, in that temperature independent thermal properties are used and radial conduction across the tile face is neglected. The latter effect would indeed lead to a higher temperature in the far SOL than anticipated with the 1-D conduction model, giving the appearance of a high heat flux. Simple estimates for ATJ-type graphite have suggested that such 2-D effects become important for time scales on the order of ~2 sec[22], *i.e.* much longer than the < 50ms of this experiment.

Secondly, we consider the impact of core and divertor radiation on the measured heat flux profile, and conclude that radiative heating of the tiles is unlikely to lead to the long decay lengths measured in the far SOL. In concept, if the heat flux due to radiation were comparable to parallel heat flow, it would cause a longer λ_q than the expected from the two-point model (equation 7). The NSTX divertor bolometer currently has three vertically resolved channels in the X-point region as shown in Fig. 1; radial resolution of the radiating region is not possible with this system. To estimate radiative heating effect on the outer lower divertor tile, we assume two cases of radiating shell (see Fig. 7); 1) Take the X-point as the radial location of the emitting volume in order to take an average over inner and outer divertor legs[29, 30]. This is a generally conservative assumption because the radiation from the inner divertor region is generally stronger than from

the outer, as measured in several unpumped diverted tokamaks[31], 2) Take the outer leg as a solely responsible radiating region. This is regarded as an even more conservative assumption in order to see the 'upper limit' of the radiation effect on the IR heat flux profile. Also assumed is that the radiation shell has a uniform radiation power over its entire surface for both cases. Taking account of toroidal extension of the radiation shell, these assumptions yield a divertor radiated power of ~ 70 kW. At most 50% of this power would be incident on the outer side, out of which at most 50% would go to the lower side. We thus expect that not more than 25% of the total radiated power would be used to heat the outer lower divertor tile, *i.e.* ~18 kW. We then estimate heat flux profile due to this radiation power, based on the average distance of the radiating shell from each radial point on the tile surface. This analysis leads to a heat flux profile decreasing with the distance from the separatrix toward the wall, *i.e.* 33 kW/m^2 at the separatrix and ~5 kW/m^2 at R-R_{sep}=8 cm. In addition, the core bolometer indicates a total of 160 kW of radiated power. However, only ~5 % of the total radiation is expected to go to the outer lower divertor tiles from solid angle considerations, which corresponds to ~8 kW. This could be incident on the outer lower tile with surface area ~1.3 m^2, leading to a heat flux of ~6 kW/m^2. In sum, the radiative heat flux profile from the divertor and the core would be only less than 10 % of the measured IR heat flux profile over the entire SOL. If we subtract this radiative contribution from the total heat flux profile and re-fit the profile, we obtain λ_q =9.2 cm (case 1 above) and λ_q =8.5 cm (case 2), similar to the uncorrected λ_q =9.3 cm. Therefore, the radiative tile heating is not thought to be the cause of the observed discrepancy.

The third possibility is that the ion heat flux to the target significantly exceeds the electron heat flux in the far SOL. Here both the ion density and temperature scale lengths would have to substantially exceed the electron scale lengths in the far SOL, which would imply the breakdown of quasi-neutrality. If the ion density decay length is longer than the measured λ_q, *i.e.* $\lambda_{ni} > 9.3$ cm, we can see that λ_q^i will be $\lambda_q^i > 9.3\,\mathrm{cm}$ (from equation 7, assuming $\lambda_{Ti} \to \infty$). As was shown

above, λ_q is $\lambda_q^e < \lambda_q < \lambda_q^i$, this can lead to a large λ_q as is observed experimentally. However, currently there is no ion density data for the NSTX SOL plasmas, and this conjecture needs to be investigated with new diagnostics in the future.

Lastly, we consider the possibility of fast ion contribution to the heat flux profile, for example from the injected neutral beam. This could, in principle, produce a very broad heat flux profile and contribute to the observed long tail in the far SOL. The beam ion orbit dynamics in NSTX usually does not allow for a significant fraction of ions to be directly lost to the target, but is lost and transfer energy around the midplane through collisions[32]. It would then reach the target via parallel transport. If the fast ion contribution is indeed significant, it would produce a difference in the heat flux profile between just before and after an NBI power switch. Our present IR camera is not ideal for this investigation because of its rather slow temporal resolution (~33ms). However, as one IR time frame presently covers only ~one beam slowing down time, we expect that the power from the core plasma across the separatrix would not be very different and any difference in the heat flux profile between two consecutive IR time frames with the NBI power switch time centered would be due to the contribution from the fast ions. IR heat flux profiles have been investigated for such shots and are shown very similar. Therefore, it does not appear that the fast ion species contributes to the broad heat flux profile in the far SOL at least for our present IR measurement with 33ms temporal resolution.

III. Effect of ELMs and turbulent blobs on the profile comparison

As discussed in section II A, the T_e profile in Fig. 4 shows a significant scatter due to the effects of ELMs and blobs on the raw I-V characteristic curves. We have investigated the effect of these transients on the T_e profile by comparing profiles from Thomson scattering (TS) and the probe. λ_{Te} from the TS measurement (=0.7cm) is shorter than the one from the probe

measurement (=1.1cm) by a factor of ~1.6. This is believed to be caused by the difference in the temporal resolution between the two diagnostics. The TS is an instantaneous measurement and therefore catches an ELM or turbulent blob only when its line of sight intersects with the ELM/blob filament. On the other hand, the swept probe measurement is continuous and is affected by filaments more substantially because of its higher probability of catching them during the sweeping period of 0.5ms. Therefore, the probe measurement conceptually represents the 'time-averaged' T_e profile and includes the effect of ELM/blob filaments, leading to a longer λ_{Te}. On the other hand, the TS measurement mostly misses the ELMs and blobs, except in the 'very near' SOL ($0 < R\text{-}R_{sep} < 1$cm) where ELMs/blob filaments are commonly present, and represents the inter-ELM T_e profile for $R\text{-}R_{sep} > 1$cm. This leads to shorter λ_{Te} shown in plot (b) of Fig. 8.

We have further investigated this issue by eliminating the effect of ELMs and blobs on the probe T_e profile, by removing the affected portions from the raw I-V curve data. This was made easier by making use of I_{sat}^{+} data from a separate I_{sat}^{+} probe which is constantly biased to -170V. By comparing the swept probe data with the I_{sat}^{+} probe data, we could determine the ELM affected portions to be removed from the raw I-V curve data. The probe T_e profile then becomes much less scattered and narrower with λ_{Te}=0.6cm, very similar to the λ_{Te}=0.7cm from the TS measurement. This is shown in plot (a) of Fig. 8.

The time frame of the IR measurement, however, is 33 ms and thus averages over these ELMs and turbulence. Note that comparison between the upstream T_e SOL width and the target heat flux SOL width presented in this paper was made by using the T_e measurement from the probe and the heat flux measurement from the IR camera. Therefore, the issue of comparing T_e and heat flux profiles during and between ELMs and turbulent blobs has not been fully addressed. That is, a fluctuating T_e profile due to these transient phenomena should be compared with the corresponding heat flux profile. This is particularly important because of the strong dependence on T_e to the 7/2 power, which makes obtaining the average T_e profile that is most appropriate for

comparison to the heat flux profile a non-linear problem when we include transient data in the measured profiles. In order to solve this problem correctly we need a measurement of T_e and heat flux profiles with a time scale fast enough to separate steady state and transient profiles, which is presently not available in NSTX. However, a fast IR camera with measurement frequency of up to 20kHz is being prepared for use from the next campaign. This is anticipated to be able to resolve, along with the 'w/ and w/o ELMs and blobs' technique in the probe data analysis described above, the issue more precisely.

IV. Summary and Conclusions

The λ_{Te}/λ_q ratio in the near SOL (R-R_{sep} < 2.5cm) was measured by fitting the profile data to: 1) a simple exponential and 2) an offset exponential, with values of 2.29 and 1.52 obtained from those functions respectively. The baseline value of the offset exponential profile can be interpreted as a result of fast radial intermittent transport. The above ratios are relatively close to calculations from a simple parallel heat conduction model, the so-called two-point SOL model, which predict values of 3.5 and 2.05 for the simple and offset exponential profiles respectively. The remaining discrepancy might be due to measurement errors or oversimplifying assumptions in the two-point model such as negligible parallel convection and equal electron and ion temperatures. In fact, the assumption of T_i=T_e can be inaccurate and T_i/T_e~2 or so is often found in the SOL[33, 34]. However, due to the very large electron conduction coefficient (κ_{0e}~2000 for hydrogenic plasmas) compared to the ion (κ_{0i} ~60), ions with T_i=2T_e would only conduct parallel heat flux a factor of ~1/6 smaller than the electrons along the SOL, assuming the same parallel gradient of T_e and T_i (see equation 1). Therefore, the contribution of parallel ion conduction to the total heat flux is expected to be small.

In the far SOL, we calculate the heat transport to be in the sheath-limited regime. The T_e, n_e, and heat flux profile data are fitted to a simple exponential form (excluding the near SOL),

obtaining that the measured λ_q is 9.3 cm, while the expected from the two-point model is $2.7 < \lambda_q < 3.9$ cm, *i.e.* the measurement being a factor of 2.4 to 3.4 larger than the expected. The reason for this discrepancy is unclear and the subject of future work, although our estimates suggest that 2-D conduction across tile surfaces, radiative heat flux to the tile surfaces, and contribution from the fast ion components to the heat flux profile are unlikely to result in the large measured values of λ_q. In principle, a significantly longer ion heat flux scale length than the electron scale length perhaps combined with long λ_{ni} and λ_{Ti} could lead to a large λ_q as observed.

Acknowledgements

The Authors would like to thank the NSTX research team and the UCSD engineering staff. This work was supported by the US Department of Energy, contract numbers DE-FG02-03ER54731, DE-AC02-76CH03073, DE-AC05-00OR22725, and DE-AC52-07NA27344.

References

[1] ITER Physics Basis Editors, Nucl. Fusion **39**, 2137-2664 (1999)

[2] Progress in ITER Physics Basis Editors, Nucl. Fusion **47**, S1-S413 (2007)

[3] J.W. Connor, G.F. Counsell, S.K. Erents, S.J. Fielding, B. LaBombard, K. Morel, Nucl. Fusion **39**, 169 (1999)

[4] W. Fundamenski, R.A. Pitts, G.F. Matthews, V. Riccardo, S. Sipila, Nucl. Fusion **45**, 950 (2005)

[5] J-W. Ahn, G.F. Counsell, A. Kirk, Plasma Phys. Control. Fusion **48**, 1077 (2006)

[6] A.W. Leonard, M.A. Mahdavi, S.L. Allen, N.H. Brooks, M.E. Fenstermacher, D.N. Hill, C.J. Lasnier, R. Maingi, G.D. Porter, T.W. Petrie, J.G. Watkins, and W.P. West, Phys. Rev. Lett. **78**, 4769 (1997)

[7] J.A. Boedo, G.D. Porter, M J. Schaffer, R. Lehmer, R.A. Moyer, J.G. Watkins, T.E. Evans, C.J. Lasnier, A.W. Leonard, and S.L. Allen, Phys. Plasmas **5**, 4305 (1998)

[8] B. LaBombard, M.V. Umansky, R.L. Boivin, J.A. Goetz, J. Hughes, B. Lipschultz, D. Mossessian, C.S. Pitcher, J.L. Terry, Alcator Group. Nucl. Fusion **40**, 2041 (2000)

[9] B. LaBombard, M. Greenwald, R.L. Boivin, B. Carreras, J. Hughes, B. Lipschultz, D. Mossessian, C.S. Pitcher, J.L. Terry, S.J. Zweben, and Alcartor C-Mod Team, *Fusion Energy 2002, Proceedings of the 19th International Conference, Lyon, France* (IAEA, Vienna, 2002)

[10] M. Ali. Mahdavi, J.C. DeBoo, C.L. Hsieh, N.Ohyabu, R.D. Stambaugh, and J.C. Wesley, Phys. Rev. Lett. **47**, 1602 (1981)

[11] K. Borrass, Nucl. Fusion **31**, 1035 (1991)

[12] P.C. Stangeby, *The Plasma Boundary of Magnetic Fusion Devices* (Institute of Physics Publishing, Bristol and Philadelphia, 2000)

[13] A. Kallenbach, N. Asakura, A. Kirk, A. Korotkov, M.A. Mahdavi, D. Mossessian, G.D. Porter, J. of Nucl. Mater. **337-339**, 381 (2005)

[14] W. Fundamenski, S. Sipila and JET-EFDA contributors, Nucl. Fusion **44**, 20 (2004)

[15] J.A. Boedo, D.L. Rudakov, R.A. Moyer, G.R. McKee, R.J. Colchin, M.J. Schaffer, P.G. Stangeby, W.P. West, S.L. Allen, T.E. Evans, R.J. Fonck, E.M. Hollmann, S. Krasheninnikov, A.W. Leonard, W. Nevins, M.A. Mahdavi, G.D. Porter, G.R. Tynan, G.D.Whyte, and X. Xu, Phys. Plasmas **10**, 1670 (2003)

[16] D.L. Rudakov, J.A. Boedo, R.A. Moyer, P.C. Stangeby, J.G. Watkins, D.G. Whyte, L. Zeng, N.H. Brooks, R.P. Doerner, T.E. Evans, M.E. Fenstermacher, M. Groth, E.M. Hollmann, S.I. Krasheninnikov, C.J. Lasnier, A.W. Leonard, M.A. Mahdavi, G.R. McKee, A.G. McLean, A. Yu. Pigarov, W.R. Wampler, G. Wang, W.P. West and C.P.C. Wong, Nucl. Fusion **45**, 1589 (2005)

[17] M. Ono, S.M. Kaye, Y.-K.M. Peng, G. Barnes, W. Blanchard, M.D. Carter, J. Chrzanowski, L. Dudek, R. Ewig, D. Gates, R.E. Hatcher, T. Jarboe, S.C. Jardin, D. Johnson, R. Kaita, M. Kalish, C.E. Kessel, H.W. Kugel, R. Maingi, R. Majeski, J. Manickam, B. McCormack, J. Menard, D.

Mueller, B.A. Nelson, B.E. Nelson, C. Neumeyer, G. Oliaro, F. Paoletti, R. Parsells, E. Perry, N. Pomphrey, S. Ramakrishnan, R. Raman, G. Rewoldt, J. Robinson, A.L. Roquemore, P. Ryan, S. Sabbagh, D. Swain, E.J. Synakowski, M. Viola, M. Williams, J.R. Wilson and NSTX Team, Nucl. Fusion **40**, 557 (2000)

[18] S.M. Kaye, M.G. Bell, R.E. Bell, S. Bernabei, J. Bialek, T. Biewer, W. Blanchard, J. Boedo, C. Bush, M.D. Carter, W. Choe, N. Crocker, D.S. Darrow, W. Davis, L. Delgado-Aparicio, S. Diem, J. Ferron, A. Field, J. Foley, E.D. Fredrickson, D.A. Gates, T. Gibney, R. Harvey, R.E. Hatcher, W. Heidbrink, K. Hill, J.C. Hosea, T.R. Jarboe, D.W. Johnson, R. Kaita, C. Kessel, S. Kubota, H.W. Kugel, J. Lawson, B.P. LeBlanc, K.C. Lee, F. Levinton, R. Maingi, J. Manickam, R. Maqueda, R. Marsala, D. Mastrovito, T.K. Mau, S.S. Medley, J. Menard, H. Meyer, D.R. Mikkelsen, D. Mueller, T. Munsat, B.A. Nelson, C. Neumeyer, N. Nishino, M. Ono, H. Park, W. Park, S. Paul, T. Peebles, M. Peng, C. Phillips, A. Pigarov, R. Pinsker, A. Ram, S. Ramakrishnan, R. Raman, D. Rasmussen, M. Redi, M. Rensink, G. Rewoldt, J. Robinson, P. Roney, A.L. Roquemore, E. Ruskov, P. Ryan, S.A. Sabbagh, H. Schneider, C.H. Skinner, D.R. Smith, A. Sontag, V. Soukhanovskii, T. Stevenson, D. Stotler, B. Stratton, D. Stutman, D. Swain, E. Synakowski, Y. Takase, G. Taylor, K. Tritz, A. von Halle, M. Wade, R. White, J. Wilgen, M. Williams, J.R. Wilson, W. Zhu, S.J. Zweben, R. Akers, P. Beiersdorfer, R. Betti, T. Bigelow, M. Bitter, P. Bonoli, C. Bourdelle, C.S. Chang, J. Chrzanowski, C. Domier, L. Dudek, P.C. Efthimion, M. Finkenthal, E. Fredd, G.Y. Fu, A. Glasser, R.J. Goldston, N.L. Greenough, L.R. Grisham, N. Gorelenkov, L. Guazzotto, R.J. Hawryluk, J. Hogan, W. Houlberg, D. Humphreys, F. Jaeger, M. Kalish, S. Krasheninnikov, L.L. Lao, J. Lawrence, J. Leuer, D. Liu, N.C. Luhmann, E. Mazzucato, G. Oliaro, D. Pacella, R. Parsells, M. Schaffer, I. Semenov, K.C. Shaing, M.A. Shapiro, K. Shinohara, P. Sichta, X. Tang, R. Vero, D. Walker and W. Wampler, Nucl. Fusion **45**, S168 (2005)

[19] J.A. Boedo, Rev. Sci. Instrum., Submitted to Review of Scientific Instruments (2008)

[20] R. Maingi, C.E. Bush, R. Kaita, H.W. Kugel, A.L. Roquemore, S.F. Paul, V.A. Soukhanovskii, NSTX Team, J. of Nucl. Mater. **363-365**, 196 (2007)

[21] R. Maingi, K. Tritz, E.D. Fredrickson, J.E. Menard, S.A. Sabbagh, D. Stutman, M.G. Bell, R.E. Bell, C.E. Bush, D.A. Gates, D.W. Johnson, R. Kaita, S.M. Kaye, H.W. Kugel, B.P. LeBlanc, D. Mueller, R. Raman, A.L. Roquemore and V.A. Soukhanovskii, Nucl. Fusion **45**, 264 (2005)

[22] C.J. Lasnier, D.N. Hill, T.W. Petrie, A.W. Leonard, T.E. Evans and R. Maingi, Nucl. Fusion **38**, 1225 (1998)

[23] L.L. Lao, Nucl. Fusion 25 (1985) 1611,

[24] S.A. Sabbagh, S.M. Kaye, J. Menard, F. Paoletti, M. Bell, R.E. Bell, J.M. Bialek, M. Bitter, E.D. Fredrickson, D.A. Gates, A.H. Glasser, H. Kugel, L.L. Lao, B.P. LeBlanc, R. Maingi, R.J. Maqueda, E. Mazzucato, D. Mueller, M. Ono, S.F. Paul, M. Peng, C.H. Skinner, D. Stutman, G.A. Wurden, W. Zhu and NSTX Research Team, Nucl. Fusion **41** (2001) 1601

[25] J.E. Menard, Private communication (2007)

[26] S.K. Erents, P.C. Stangeby, B. Labombard, J.D. Elder, W. Fundamenski, Nucl. Fusion **40**, 295 (2000)

[27] H.Y. Guo, Contrib. to Plasma Phys. **36**, S81 (1996)

[28] R.A. Pitts, Contrib. to Plasma Phys. **36**, S87 (1996)

[29] S.F. Paul, R. Maingi, V. Soukhanovskii, S.M. Kaye, H.W. Kugel, J. of Nucl. Mater. **337-339**, 251 (2005)

[30] S.F. Paul, Private communication (2008)

[31] A.W. Leonard, , C.J. Lasnier, J.W. Cuthbertson, T.E. Evans, M.E. Fenstermacher, D.N. Hill, R.A. Jong, W.H. Meyer, T.W. Petrie, G.D. Porter, J. Nucl. Materials **220-222**, 325 (1995)

[32] D. Darrow, Private communication (2008)

[33] A. Kirk, W. Fundamenski, J-W. Ahn, and G.F. Counsell, Plasma Phys. Control. Fusion **45**, 1445 (2003)

[34] A. Kirk, G.F. Counsell, W. Fundamenski, J-W. Ahn, D. Taylor, M. J. Walsh, Y. Yang, and the MAST Team, Plasma Phys. Control. Fusion **46**, 1591 (2004)

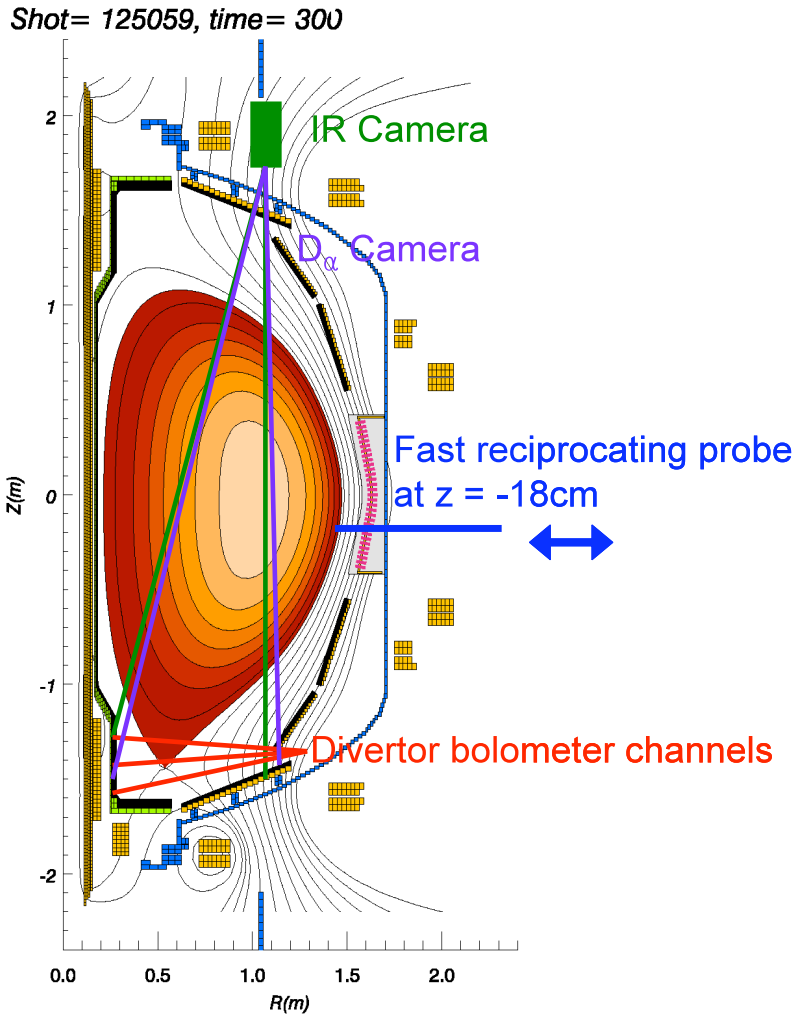

FIG. 1. Magnetic equilibrium reconstruction of NSTX shot 125059 with various diagnostics channels overlaid.

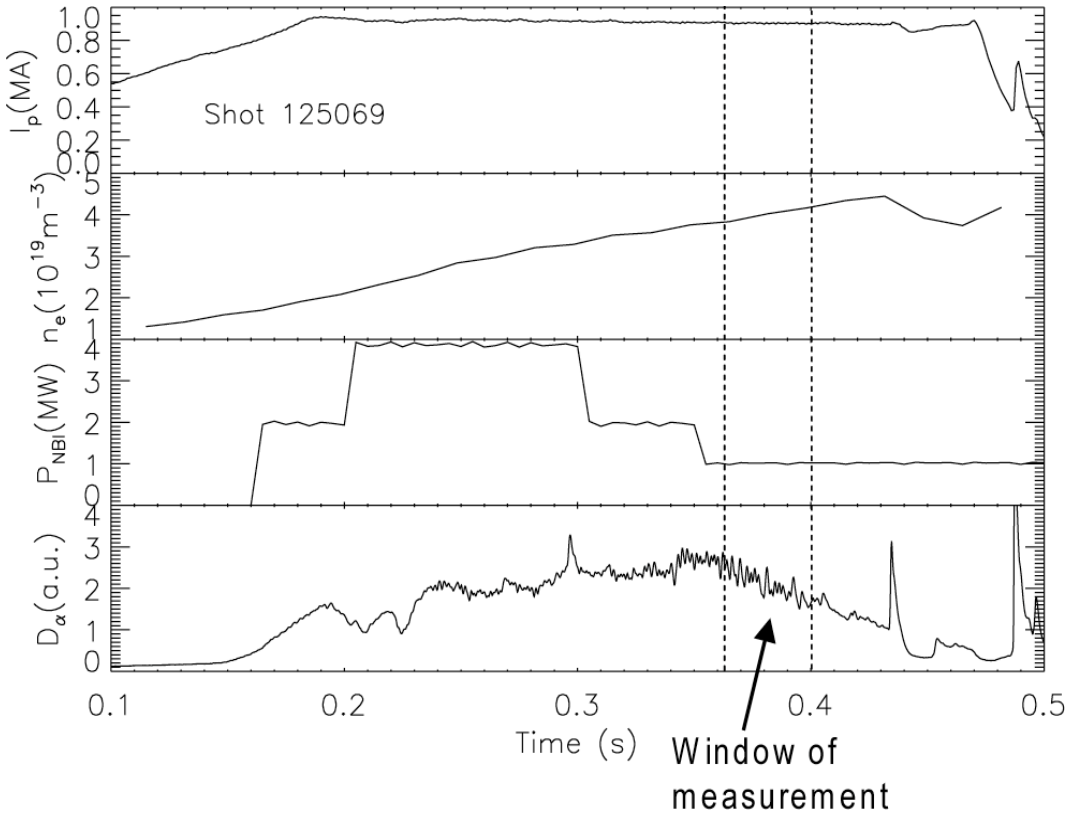

FIG. 2. Time trace of various discharge parameters: a) plasma current, b) line averaged density, c) injected NBI power, and d) D_α signal for lower divertor. The sky colored window indicates the time period of probe and IR measurements.

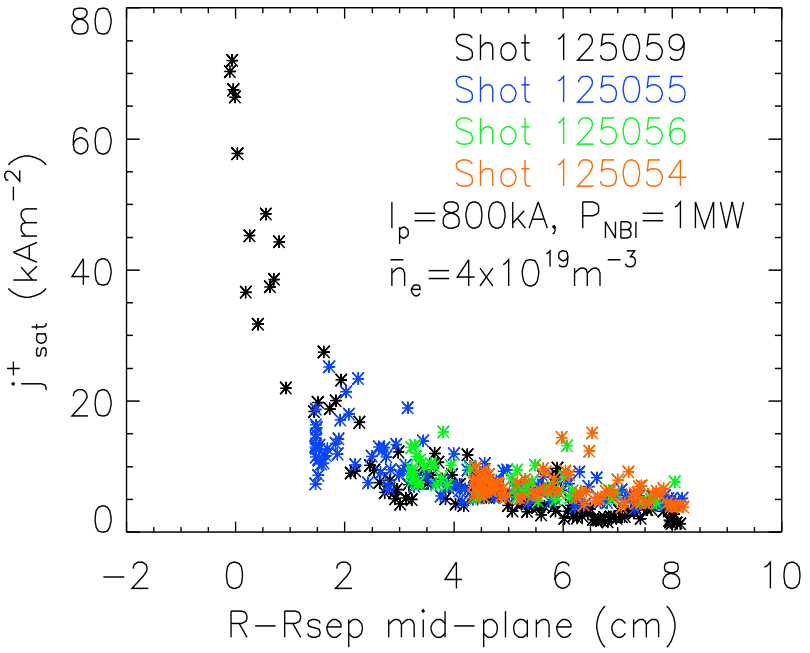

FIG. 3. Profiles of ion saturation current density (j^+_{sat}) as a function of R-R_{sep} (mapped to the mid-plane), from the fast reciprocating probe measurement for 4 nominally identical shots with different maximum probe penetration.

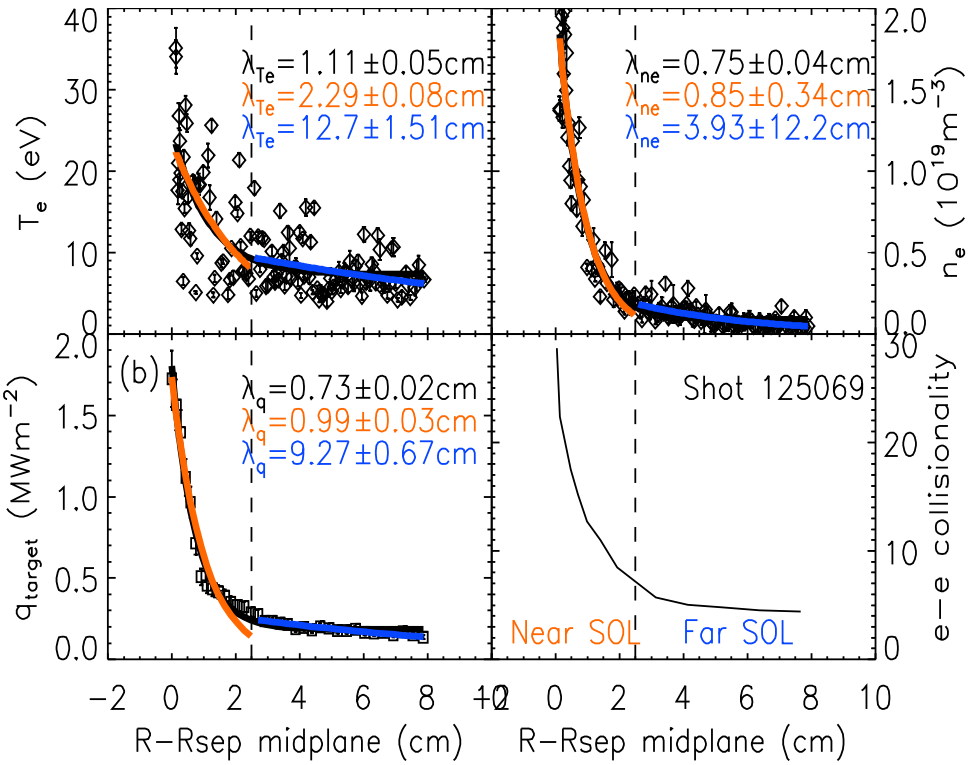

FIG. 4. Measured T_e, n_e (by fast reciprocating probe at z = -17.3cm), and q_{target} (by IR camera at the lower divertor target) profiles, as well as the calculated SOL electron-electron collisionality profile, with all profiles mapped to the mid-plane. The black fitting lines are from the offset exponential function for the whole profiles, while the orange and blue lines are from the simple exponential function in the near and far SOL regions, respectively. Statistical error bars on the decay lengths are also indicated.

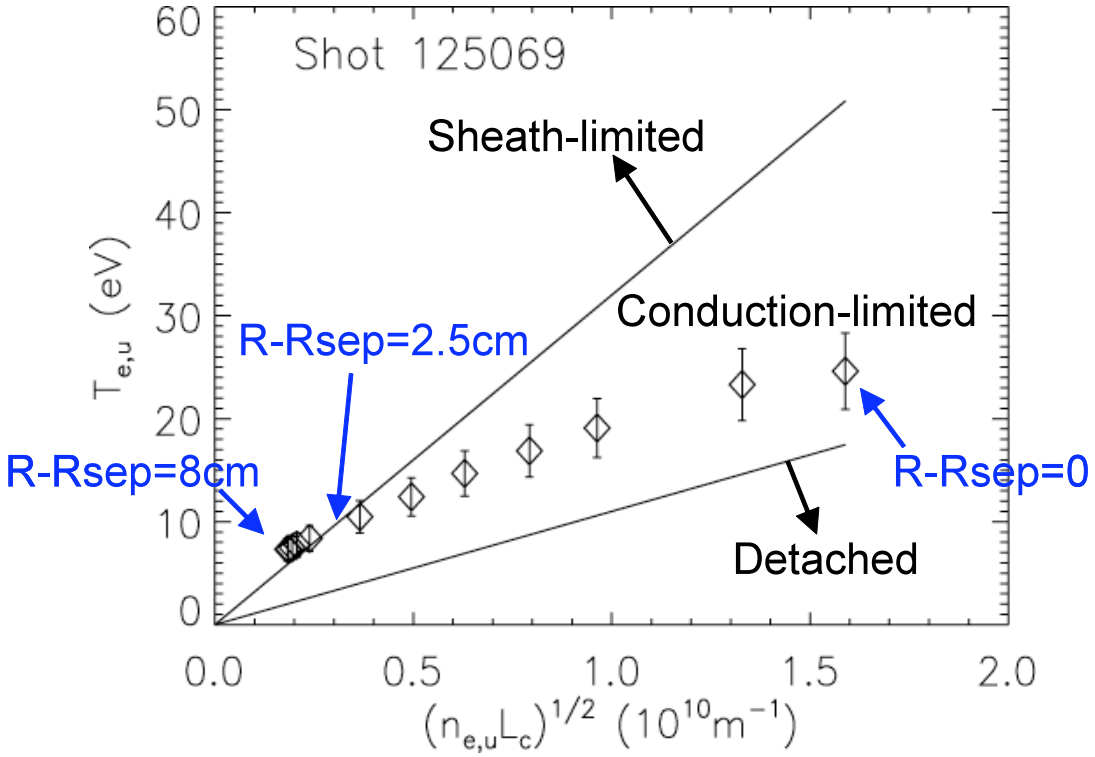

FIG. 5. $T_{e,u}$ versus $(n_{e,u}L_c)^{1/2}$ for the NSTX SOL data shown in Fig. 4, where $T_{e,u}$ and $n_{e,u}$ are 'upstream' T_e and n_e values measured by the reciprocating probe. The solid lines are given by a two-point model analysis[26]. Note that the NSTX upstream SOL plasma (at the mid-plane) enters the sheath-limited regime at ~2.5cm away from the separatrix.

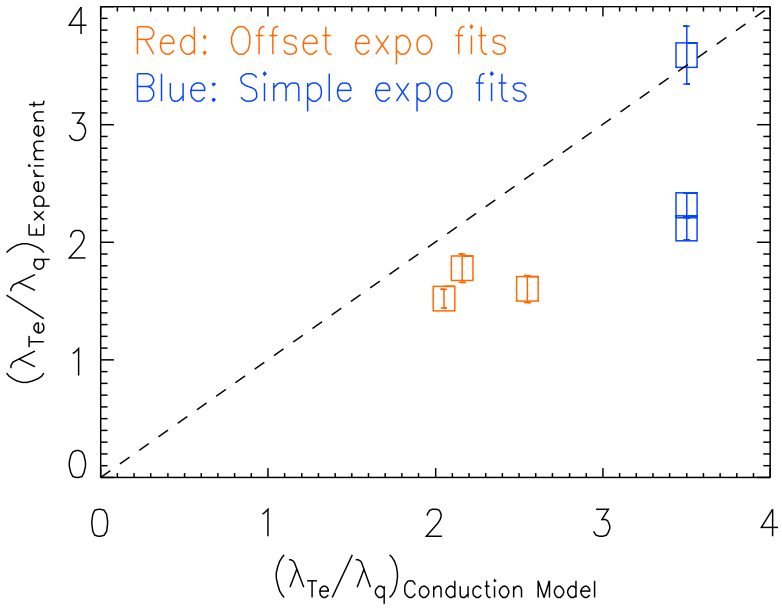

FIG. 6. Near SOL λ_{Te}/λ_q from the experiment and electron conduction model for three different discharges. Note that experimental values tend to be smaller than values from the conduction model by 25-30%.

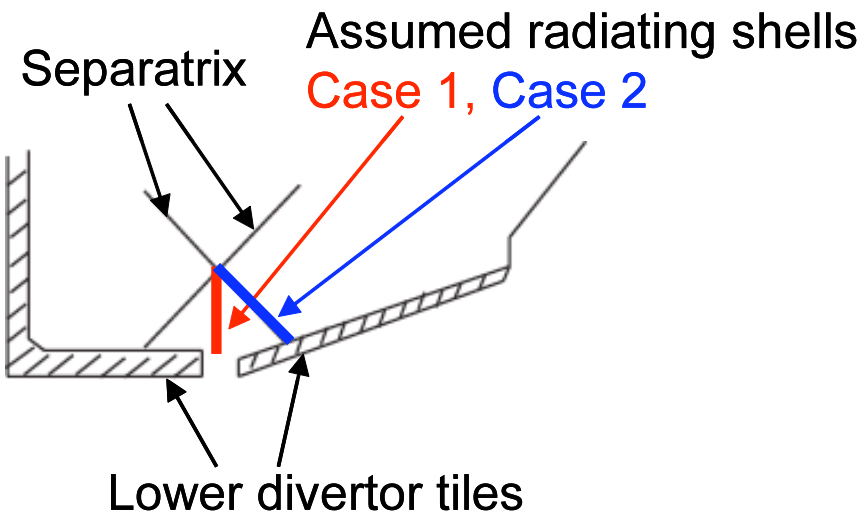

FIG. 7. Geometry of simplified divertor radiation zones assumed to estimate contribution of the radiation power to the measured IR heat flux profile.

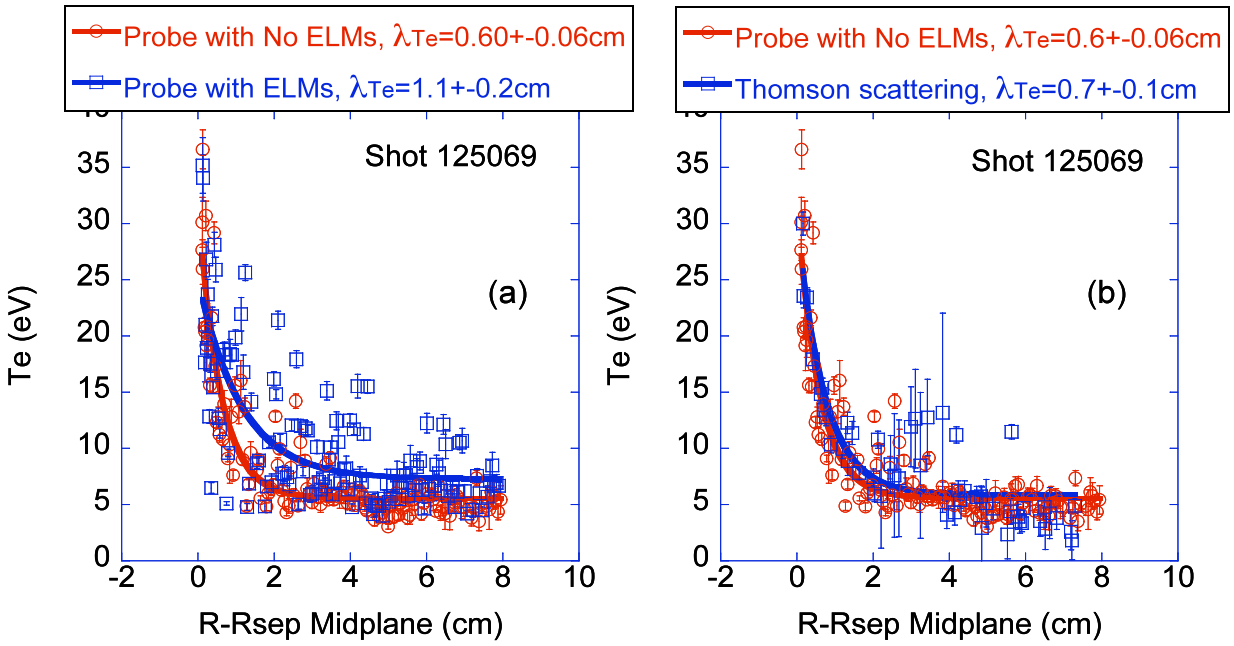

FIG. 8. (a) λ_{Te} with and without ELMs from the probe measurement, (b) λ_{Te} from the probe measurement without ELMs and from the TS measurement. Here, probe data 'without ELMs' means that the ELM affected portions of I-V characteristics curve were removed before the fitting process.